Synthesis, Characterization, and Tunable Adsorption and Diffusion Properties of Hybrid ZIF-7-90 Frameworks

Fereshteh Rashidi, Catherine R. Blad, Christopher W. Jones, and Sankar Nair
School of Chemical and Biomolecular Engineering, Georgia Institute of Technology, Atlanta, GA 30332-0100

DOI 10.1002/aic.15102
Published online December 8, 2015 in Wiley Online Library (wileyonlinelibrary.com)

Hybrid zeolitic imidazolate frameworks (ZIFs), containing more than one type of imidazolate linker, can allow highly tunable molecular sieving and adsorption. Their crystallization becomes more challenging when the end-member (single-linker) ZIFs crystallize in different crystal systems. We demonstrate the controlled synthesis and detailed characterization of hybrid ZIF-7-90 frameworks containing linkers of ZIF-7 (rhombohedral) and ZIF-90 (cubic). ZIF-7-90 materials with SOD-type topology are obtained in three crystalline phases depending on the linker composition and synthesis technique. The effect of synthesis conditions on the activation-induced phase transition from rhombohedral to other topologies is studied. Nitrogen physisorption at 77 K and CO_2 physisorption at 273 K shows the tunability of the pore-size distribution and the framework flexibility as a function of framework composition. Measurements of water adsorption and butane isomer diffusion illustrate the tunability of diffusivity over seven orders of magnitude and control of hydrophobic to hydrophilic adsorption behavior. © 2015 American Institute of Chemical Engineers *AIChE J*, 62: 525–537, 2016

Keywords: metal-organic frameworks, mixed-linker MOFs, separation, membrane materials

Introduction

Zeolitic imidazolate frameworks (ZIFs) consist of tetrahedral metal (Zn^{2+} or Co^{2+}) sites bridged by nitrogen atoms of imidazolate linkers. ZIFs are promising materials for adsorption, membranes, sensors, and catalysis due to their high microporosity and good chemical and thermal stability.[1–6] The pore sizes of ZIFs (0.2–2 nm) allow selective sieving and recognition of molecules. ZIFs can also show dynamic structural transitions during adsorption, known as the "gate-opening" phenomenon.[5,7–9] This is attributed to rotation of the linkers that causes a sudden increase of the adsorbed amount at a very low pressure; hence ZIFs can be considered to be relatively flexible nanoporous materials vs. more rigid materials such as zeolites. This flexibility introduces significant challenges in designing ZIFs for separations of molecules of similar size. ZIF-7, ZIF-8, and ZIF-90 are three of the most well-known ZIF materials. ZIF-8 and ZIF-90 frameworks prefer to crystallize in the cubic (I-43m) SOD topology, whereas ZIF-7 prefers the rhombohedral ($R\bar{3}$) SOD topology.[2] Recent studies have shown that ZIF-7 can undergo structural transformations. Aguado et al.[9] reported a reversible phase transition from a narrow-pore to large-pore form of ZIF-7 during CO_2 adsorption. Zhao et al.[10] showed three crystalline phases of pure ZIF-7 on thermal activation to remove the solvent molecules from the pores: rhombohedral $R\bar{3}$ (ZIF-7-I), monoclinic $C2/c$ (ZIF-7-II), and triclinic $P1$ (ZIF-7-III), all with SOD topology.

Although a number of ZIF structures have been synthesized, systematic approaches to the tuning of their structural properties are also required to realize a wider platform of ZIF materials that are useful for molecular separations. Several approaches have been shown to tune and modify the properties of ZIF frameworks through chemical or structural modifications. The three primary approaches taken are postsynthesis modification,[11] solvent-assisted linker exchange,[12,13] and the mixed-linker synthesis strategy[5] to tune the microporosity of the framework, to form a different topology,[14] or to form a more efficient membranes for CO_2 capture.[15] An attractive aspect of the mixed-linker approach is the possibility of optimally tuning the properties of the ZIF for a desired function. Previously,[5,16,17] we have synthesized hybrid ZIF-8-90 and ZIF-7-8 materials by inclusion of 2-carboxyimidazole (ZIF-90 linker) and benzimidazole (ZIF-7 linker) along with 2-methylimidazole (ZIF-8 linker) during synthesis, and demonstrated control of pore size, hydrophilicity/organophilicity, and sorbate diffusion properties.

However, the synthesis and characterization of mixed-linker ZIF systems requires significant further development, especially in more challenging cases wherein the two end-member ZIFs prefer to crystallize in different crystal systems and under very different synthesis conditions. In particular, we discuss here the synthesis and characterization of ZIF-7-90 frameworks containing linkers of ZIF-7 (benzimidazole, Bz-IM) and ZIF-90 (carboxaldehyde-2-imidazole, OHC-IM). This hybrid ZIF system allows a significantly more expanded range (3.7–5 Å) of effective pore-size control in relation to the ZIF-7-8 (3.7–4 Å) and ZIF-8-90 (4–5 Å) systems. Through a detailed

Additional Supporting Information may be found in the online version of this article.

Correspondence concerning this article should be addressed to S. Nair at sankar.nair@chbe.gatech.edu.

investigation of the synthesis parameter space, we show that it is possible to synthesize ZIF-7-90 hybrids in a large range of composition, and that no single solvent system or synthesis condition can yield all the desired materials (unlike the cases of ZIF-8-90 and ZIF-7-8). Using a battery of characterization methods, we track the formation of different phases of crystalline, thermally stable, ZIF-7-90 structures that exhibit adsorption and diffusion properties different from the parent end-member frameworks. These results are valuable in the design of ZIF materials and membranes for use in separation processes.

Experimental Section

Materials

Carboxyaldehyde-2-imidazole (99%, OHC-IM), dimethylformamide (DMF), benzimidazole (99%, Bz-IM), and sodium formate (99%, $NaCO_2H$) were obtained from Alfa Aesar. $Zn(NO_3)_2{\cdot}6H_2O$ (99%) was obtained from Sigma-Aldrich. Methanol (MeOH) was obtained from HPLC. Deionized water was produced with a Thermo Scientific 7128. All materials were used without further purification.

Synthesis of ZIF-7-90 hybrids

A systematic exploration of the synthesis conditions (including of different solvents and temperatures) was carried out as described in detail below.

Single-Solvent Synthesis at High Temperature (90–140°C). (1) *MeOH solvent at 90°C*. The method previously used to grow large crystals (>100 mm) of hybrid ZIF-8-90[17] was used with a slight modification. A solution of x mmol of Bz-IM and (8-x) mmol of OHC-IM was dissolved in 40 mL of MeOH. The value x was 0–8. A mixture consisting of 0.595 g (2 mmol) of $Zn(NO_3)_2{\cdot}6H_2O$ dissolved in 40 mL MeOH was poured into the mixed linker solution. The resulting solution was heated at 90°C for 48 h in a sealed glass jar. Large crystals formed on the walls and bottom of the jar were collected and washed several times with MeOH, and then dried in an oven at 80°C. ZIF-7-90 synthesis behaves differently from ZIF-8-90 materials. The latter materials require the use of sodium formate (NaCOOH), but its use in ZIF-7-90 synthesis is found to yield amorphous materials due to its fast deprotonation of the linkers. Also, in ZIF-7-90 synthesis, crystalline phases cannot be formed in very polar solvents such as DMF or nonpolar solvent such as 1-octanol. (2) *DMF solvent at 110–140°C*. The use of an amide solvent such as DMF solvent along with high temperatures (110–140°C) and a long crystallization time are methods used by many researchers to form pure ZIF-7.[2,18] We attempted to form ZIF-7-90 materials at similar conditions in presence of both Bz-IM and OHC-IM linkers. A mixture of x mmol of Bz-IM, 1-x mmol of OHC-IM, and y mmol of $Zn(NO_3)_2{\cdot}6H_2O$ was dissolved in 20–25 mL of DMF. The values x and y were (0.7–2) mmol and (0.15–2) mmol, respectively. The resulting solution was poured in a teflon holder, sealed, and heated at 110–140°C for 48–120 h. The longer times were used at lower temperatures (110°C). The large and small crystals formed on the walls and bottom of the holder were collected and washed several times with MeOH, and then dried in an oven at 80°C. We found that the crystal size of pure ZIF-7 is dependent on x and y parameters. The higher concentrations of BZ-IM ligand and zinc lead to the formation of nanocrystals, for example, if $x=2$ and $y=2$. The large crystals (about 10 μm) are formed at lower concentration such as $x=0.7$ and $y=0.8$ at 130°C for 48 h, then. Also, the longer crystallizations period or the higher ratio of BZ-IM over zinc ($x=2$ and $y=0.15$–0.28) produce the larger crystals. Although, using above method the pure ZIF-7 crystals in different sizes can be synthesized, but ZIF-7-90 materials only can be formed in an amorphous phase.

Two-Solvent-Synthesis at Room Temperature (25°C). These crystals were synthesized using variations of the NSIC[19] method earlier reported by Thompson *et al* for the synthesis of hybrid ZIF-8-90 and ZIF-7-8 materials.[5] Four different solvent systems were used to synthesize hybrid ZIF-7-90; DMF-MeOH, DMF- H_2O, MeOH-DMF, MeOH- H_2O, and H_2O -MeOH. The two-solvent system is defined as (solvent #1 to dissolve linkers)-(solvent #2 to dissolve zinc ions). A solution of x mmol of Bz-IM, 20-x mmol of OHC-IM, and 20 mmol of $NaCO_2H$ in 50 mL of MeOH, DMF, or H_2O was prepared. The value x was varied between 0 and 20. The solution was stirred and heated at 50°C until it became clear, and then cooled down to room temperature. A solution of 5 mmol of $Zn(NO_3){\cdot}6H_2O$ in 50 mL of H_2O, DMF, or MeOH was prepared, poured into the first solution, and the resulting mixture was allowed to stir at room temperature for 1–4 h. On adding the zinc solution, fast crystallization with high yield was observed for synthesis with over 74% Bz-IM (i.e., under 26% OHC-IM) linker mole fraction. Longer crystallization times (2–4 h) with low yield were observed at lower Bz-IM loadings. ZIF crystals were collected by centrifugation at 8000 rpm for 6 min, washed in MeOH three times, and dried in an oven at 80°C.

Activation

All the ZIF-7-90 crystals formed in the single-solvent or two-solvent syntheses were activated to remove the solvent guest molecules (particularly DMF) from the micropores. The as-made crystals were soaked in MeOH at 50°C for 24 h to perform exchange of the guest solvent molecules with MeOH. The solvent-exchanged crystals were washed in fresh MeOH and collected by centrifugation, a process which was repeated thrice. They were then dried in a vacuum oven at 200°C for 24 h.

Characterization methods

XRD patterns were measured on a PANalytical X'Pert Pro diffractometer at room temperature using Cu Kα radiation of $\lambda = 0.154$ nm and a scanning range of 5–40° 2θ with low background sample holder. Solution ^{1}H-NMR measurements were performed with a Bruker 400 MHZ spectrometer after digesting the ZIF crystals in d_4-acetic acid (CD_3CO_2D). To determine the fraction of each imidazole linker in the ZIF materials, the integrated peak area of the methyl protons of Bz-IM (chemical shift 9.05 ppm) was normalized to that of the aldehyde proton of OHC-IM (9.84 ppm). The chemical shifts of both imidazole linkers were referenced to the chemical shift (2.30 ppm) of d_4-acetic acid. Thermogravimetric and decomposition analysis was performed on a Netzsch STA-409-PG thermogravimetric analyzer (TGA) and differential scanning calorimeter (DSC). Activated samples were heated from room temperature up to 900°C with a ramp rate of 10 K/min in a diluted air stream (40% air/N_2). Smoothed differential mass loss curves were analyzed to determine the decomposition temperature. Powder FT-Raman spectroscopy was performed with a Bruker Vertex 80v FTIR/RAM II FT-Raman Analyzer in open atmosphere and a He/Ne red laser (1054 nm).

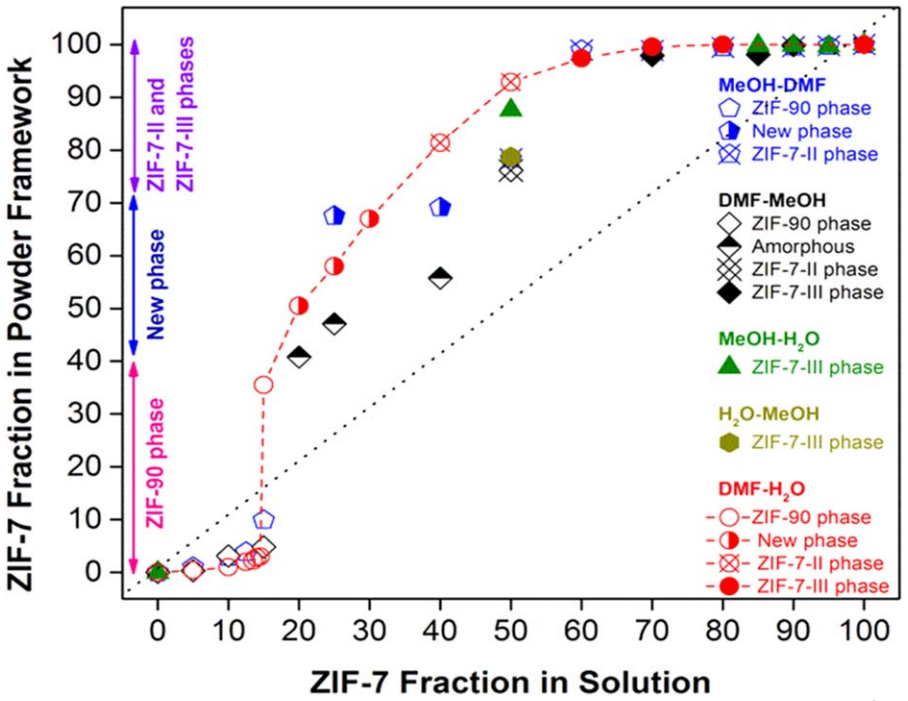

Figure 1. Composition diagram of activated hybrid ZIF-7-90 frameworks, as obtained by ^{1}H-NMR composition measurements. Crystal phases indicated on the left are discussed in detail in Figure 3.

[Color figure can be viewed in the online issue, which is available at wileyonlinelibrary.com.]

Numerical integration of FT-Raman peak areas was carried out with the instrument software. The BZ-IM and OHC-IM peaks were background-subtracted using a polynomial, and then fitted with mixed Gaussian–Lorentzian functions to obtain the integrated peak areas. Hitachi SU 8010 FESEM at 5 keV was used to observe the particle size and morphology. The sample powders were first dispersed by sonication in a filtered MeOH solution for 5 min before dropping on the SEM grids.

N_2 and CO_2 physisorption measurements were performed on a Micromeritics ASAP 2020 surface area analyzer at 77 K and 273 K, respectively. CO_2 adsorption at 273 K allowed rapid equilibration with no diffusion limitations even for the smallest pore-size materials, which are not accessible to N_2 at cryogenic temperatures. The activated samples were degassed at 200°C under vacuum for 18 h before physisorption measurements. Pore-size distributions (PSDs) of hybrid materials were calculated using the Horváth–Kawazoe (HK) model.[5,20] The BET, Langmuir, Dubinin–Radushkevich and *t*-plot micropore volume methods were also used to analyze the textural properties of the hybrid ZIFs. Water adsorption isotherms were collected using a VTI SA Vapor Sorption Analyzer (TA Instruments). Approximately 10–20 mg samples were used for each experiment. The activated samples were degassed *in situ* at 105°C for up to 9 h in an ultrapure N_2 stream. The relative vapor pressure of each adsorbate was varied between the limits of 0.01 and 0.9 in discrete steps. Equilibrium was assumed to be achieved if less than 0.003% weight change was observed in a 5-min interval.

The *n*-butane and *i*-butane transport diffusivities were measured with a volumetric (pressure decay) apparatus.[17,21,22] A known amount of ZIF sample was sealed into a 0.5 μm filter element and installed in the sample chamber. The volumes of the sample chamber and reservoir chamber are precisely known. It was determined that all our experiments satisfied the criterion for isothermal macroscopic diffusion.[22,23] The apparatus was placed in a silicone oil bath equipped with a circulator for temperature control. The activated sample was degassed under vacuum at 120°C for 12 h and then maintained for 12 h at 35°C. The vacuum was then isolated, and a known quantity of hydrocarbon gas was injected into the reservoir chamber. The valve connecting the sample and reservoir chambers was then opened. Sensitive pressure transducers attached to the sample and reservoir chambers were used to measure the pressure changes over time, occurring due to adsorption. The data were converted to uptake curves using a virial equation of state.

Results and Discussion

Composition analysis

Thompson et al.[5] showed that in the NSIC method the linker with lower solubility in the non-solvent is preferentially incorporated into the mixed-linker/hybrid ZIF framework. Therefore, the ratio of the linkers in the hybrid materials is generally different from that in the synthesis solution. Solution ^{1}H NMR is a reliable technique to quantify the relative linker fractions of Bz-IM and OHC-IM in the hybrid ZIF-7-90 crystals. Thus we established the NMR-derived composition diagram (Figure 1) to relate the linker compositions in the synthesis solution and in the ZIF framework. The diagram shows that in most cases (>15% Bz-IM in the synthesis solution), Bz-IM is incorporated into the framework with a higher fraction than it is originally present in the reactant solution, regardless of the solvent system used. Among the solvent systems, DMF-H_2O allows successful synthesis of crystalline ZIF-7-90 compositions over the widest range of Bz-IM linker fractions (15–100%). We found it difficult to synthesize ZIF-7-90 materials

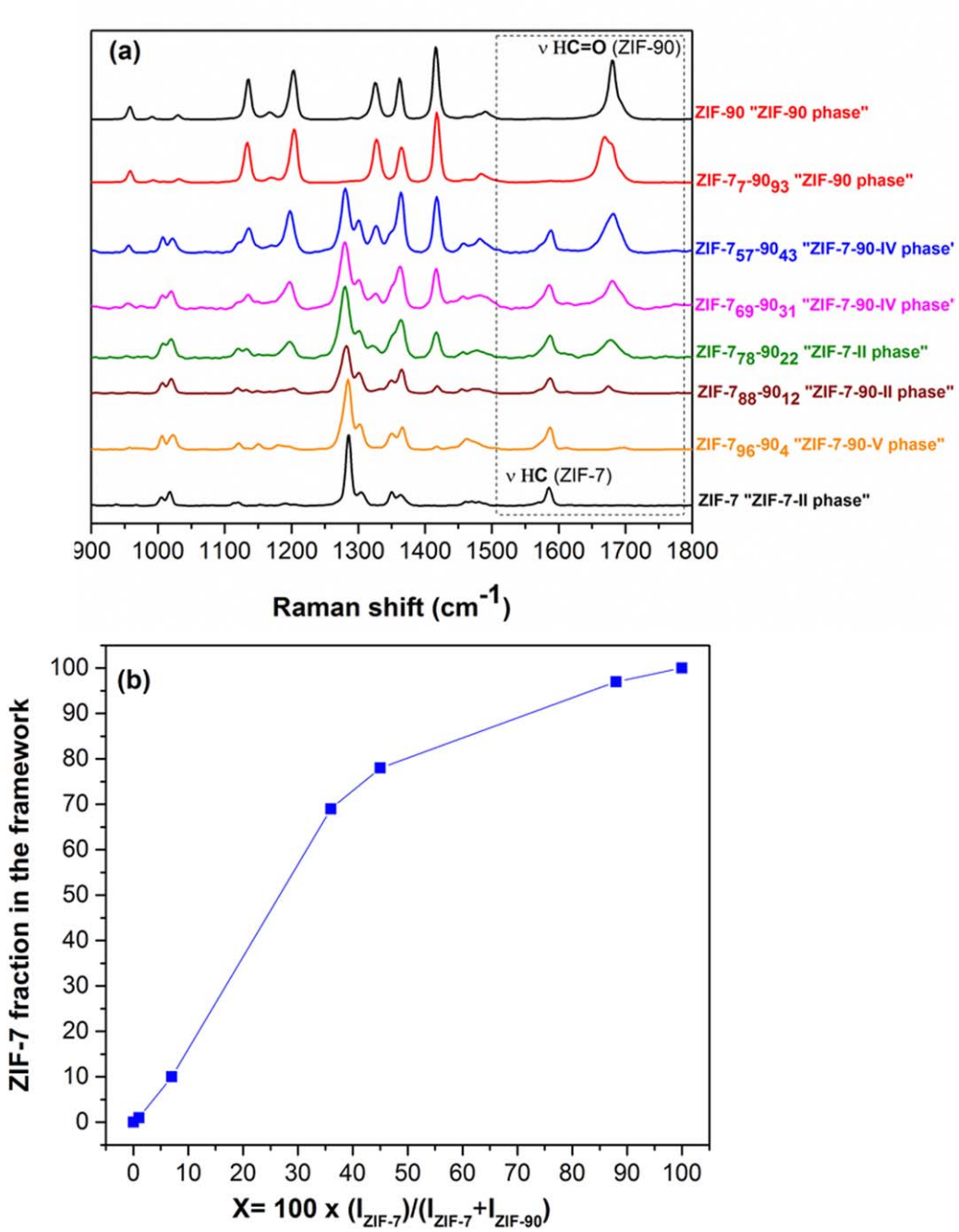

Figure 2. (a) Powder FT-Raman spectra of ZIF-7-90 hybrid framework materials and (b) Composition analysis of ZIF-7-90 hybrid crystals from FT-Raman data. The quantity $X = 100 \times I_{ZIF\text{-}7}/(I_{ZIF\text{-}7}+I_{ZIF\text{-}90})$ is obtained from the FT-Raman measurement whereas the quantity *y* is the corresponding ZIF-7 linker fraction obtained from ^{1}H-NMR.

[Color figure can be viewed in the online issue, which is available at wileyonlinelibrary.com.]

in the Bz-IM < 15% range. In this range, the MeOH-DMF solvent system yielded slightly better results than the DMF-H_2O system.

Recently, we provided direct evidence (*via* micro-Raman and powder FT-Raman spectroscopy) that crystallized ZIF-8-90 materials are true hybrids and not physical mixtures of ZIF-8 and ZIF-90 crystals.[17] However, the objective lenses mounted on our micro-Raman instrument cannot provide enough resolution to collect micro-Raman spectra for the present case of small ZIF-7-90 crystals, thus only powder FT-Raman measurements were performed on the ZIF-7-90 materials. Figure 2a shows powder FT-Raman spectra from several hybrid ZIF-7-90 materials. We use the peaks 1590 cm^{-1} (of Bz-IM) and 1680 cm^{-1} (C═O stretching vibration of OHC-Im) as signatures of the ZIF-7 and ZIF-90 linkers, respectively. In the hybrid ZIF-7-90 materials both peaks are observed due to the presences of both linkers in the framework. As the OHC-IM content increases, the intensity of the Bz-IM peaks decreases and it is eliminated in pure ZIF-90. The integrated areas ($I_{ZIF\text{-}7}$ and $I_{ZIF\text{-}90}$) of the signature peaks in each FT-Raman spectrum use the normalized quantity $X = 100 \times I_{ZIF\text{-}7}/(I_{ZIF\text{-}7}+I_{ZIF\text{-}90})$ as a measure of the percentage

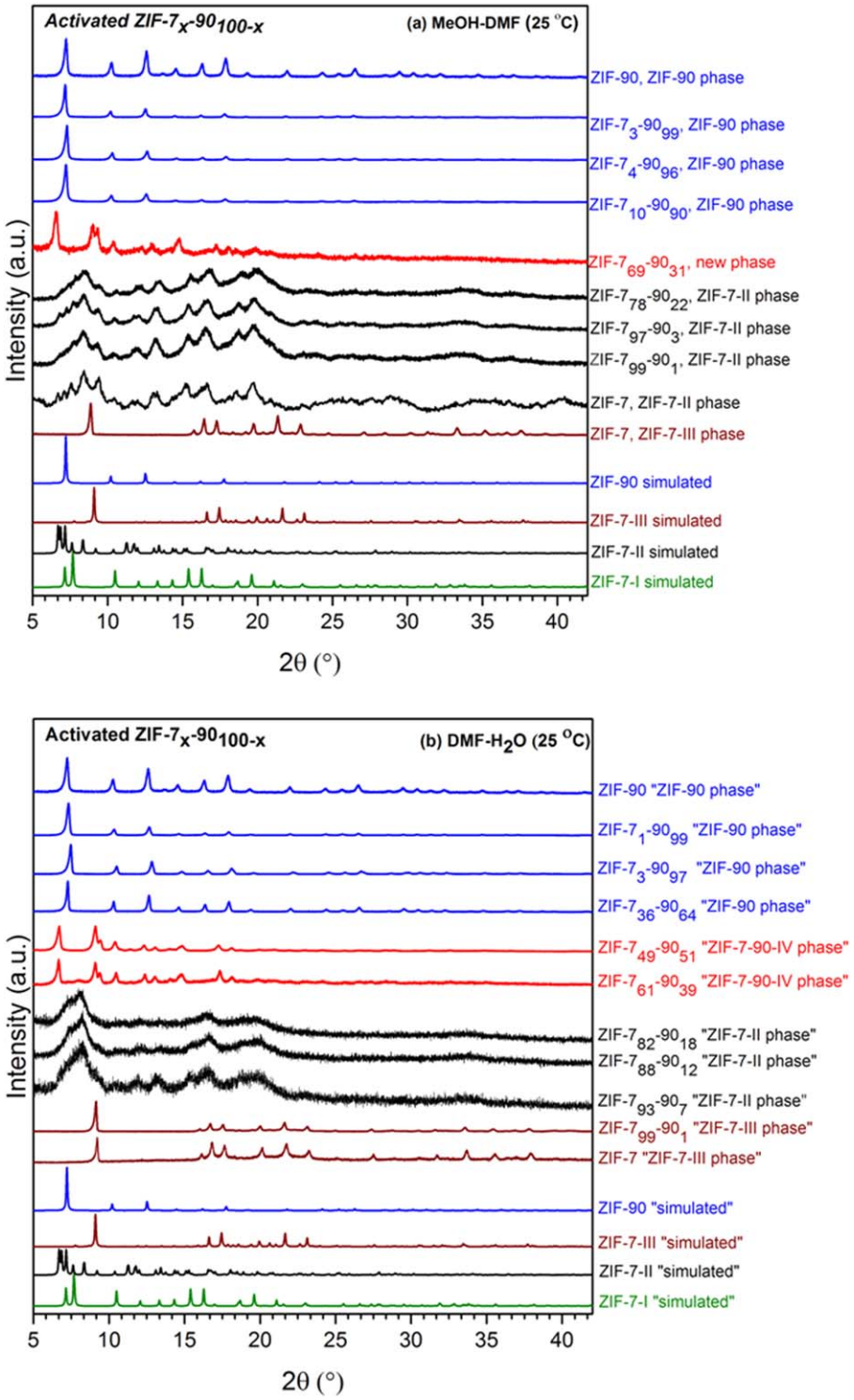

Figure 3. Powder XRD patterns of activated ZIF-7-90 hybrids synthesized in (a) DMF-H_2O and (b) MeOH-DMF. Percentages shown are determined from solution ^{1}H NMR.

[Color figure can be viewed in the online issue, which is available at wileyonlinelibrary.com.]

of ZIF-7 linkers in the framework. Because of different polarizabilities of the two characteristic linker vibrations, the quantity X is not the exact equivalent of the ZIF-7 linker fraction (x). Figure 2b plots the values of X obtained from FT-Raman measurement vs. the values of x obtained previously from ^{1}H-NMR measurements. As in the case of ZIF-8-90 hybrids, the continuous trend observed in Figure 2b indicates that the ZIF-7-90 materials are also true mixed-linker hybrids.

Crystal structure

The crystallinity and crystalline phase of the frameworks prepared in different solvent systems with different ratios of linkers were examined by XRD. Figures 3 and 4 show the XRD patterns of activated ZIF-7-90 materials, whereas Supporting Information Figure S1 shows the XRD patterns of the corresponding as-made materials. ZIF-90 is known only in the cubic (SOD) topology[5] whereas ZIF-7[18,19] may take

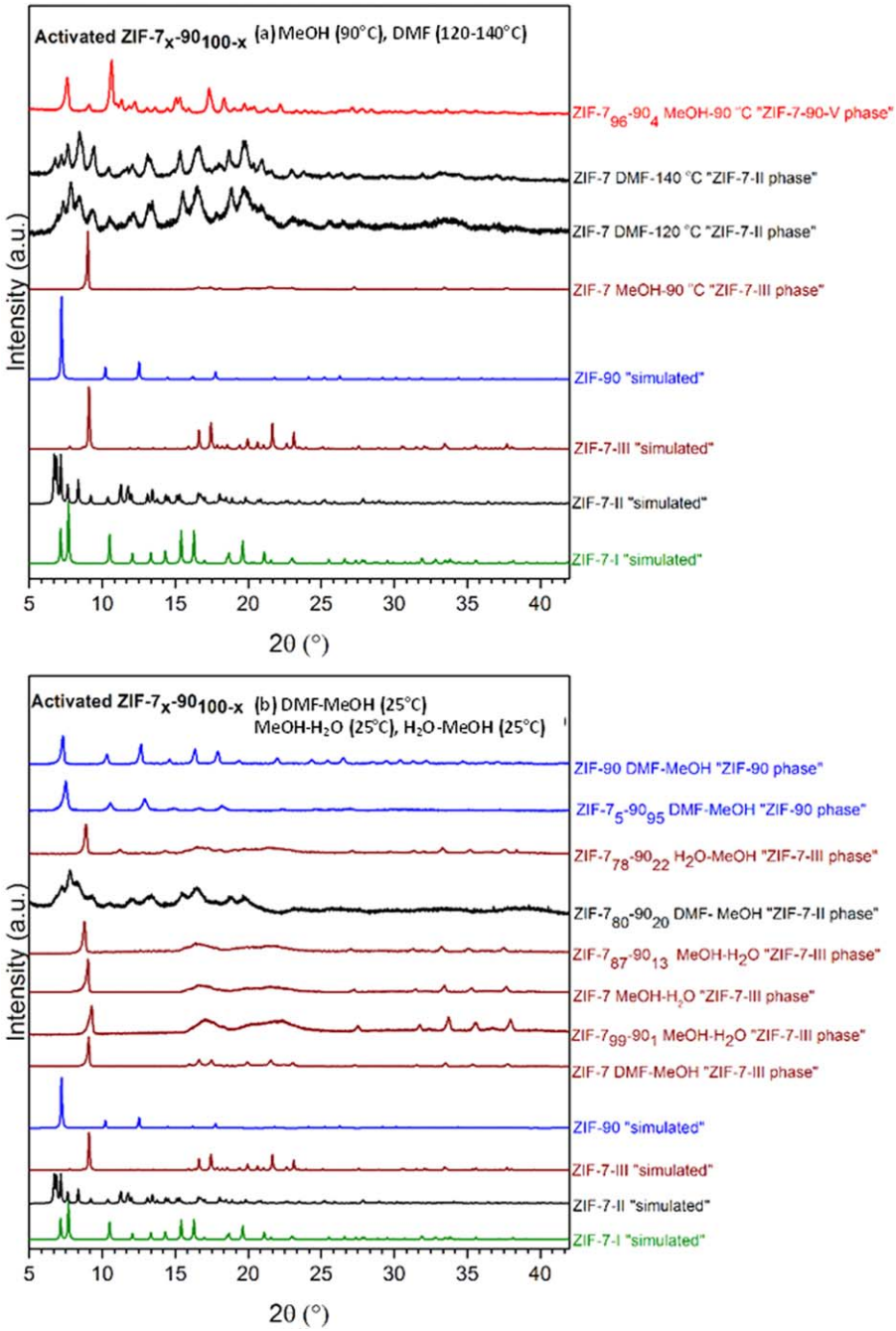

Figure 4. Powder XRD patterns of activated ZIF-7-90 hybrids synthesized in (a) DMF (120–140°C), MeOH (90°C) and (b) DMF-MeOH, MeOH-H_2O, H_2O-MeOH. Percentages shown are determined from solution ^{1}H NMR.

[Color figure can be viewed in the online issue, which is available at wileyonlinelibrary.com.]

rhombohedral (ZIF-7-I), monoclinic (ZIF-7-II), or triclinic (ZIF-7-III) forms depending on the presence of guest molecules. Supporting Information Figure S1 shows that as-made ZIF-7-90 materials synthesized in DMF-H_2O, MeOH-DMF and DMF-MeOH favor the rhombohedral ZIF-7-I phase above 70% Bz-IM loading. After activation, the hybrid materials in the 70–97% Bz-IM range transition to the monoclinic ZIF-7-II phase in MeOH-DMF (Figure 3a), whereas the triclinic ZIF-7-III phase is formed by frameworks synthesized in DMF-H_2O with 97–100% Bz-IM loading (Figure 3b).

However, between 40% and 70% Bz-IM loading there is a new phase formed by the mixed-linker ZIF-7-90 materials synthesized in DMF-H_2O and MeOH-DMF solvent systems at room temperature (Figures 3a, b). This phase (which we refer to as "ZIF-7-90-IV") has not been reported previously for either pure ZIF-7 or ZIF-90. Its first diffraction peak is at 7° 2θ, indicating that it is also a microporous material. The new phase is also highly stable and does not undergo any phase transition after activation at 200°C. The methanol solvent system at 90°C yields another new and apparently microporous phase (Figure 4a, "ZIF-7-90-V") which is different from that shown in Figure 3. All frameworks up to 40% Bz-IM loading display the cubic phase of ZIF-90 before and after activation. This is in good agreement with our previous data for hybrid

ZIF-7-8 materials.[5] Also, all as-made hybrid ZIF-7-90 materials formed in MeOH-H_2O and H_2O-MeOH systems take the ZIF-7-III phase before and after activation (Figure 4b). Finally, the XRD patterns do not indicate formation of physical mixtures of ZIF-7 and ZIF-90 materials in any of the syntheses.

Morphology and crystal-size distribution

FESEM imaging was used to examine the morphology and crystal-size distribution as a function of the synthesis conditions. Figure 5 shows representative SEM images of the activated ZIF-7-90 hybrid materials with different Bz-IM loadings synthesized at different conditions, whereas Supporting Information Figure S2 shows the corresponding crystal-size distributions (CSDs) obtained from large-area SEM images. Figure 5 shows that each crystalline phase exhibits a well-defined morphology. The morphology of the pure ZIF-7 crystals appears to be strongly dependent on the crystalline phase formed. Very large pure ZIF-7 crystals formed either at room temperature or at 90°C (Figures 5a, b) take the ZIF-7-III phase after activation. Within this set, the as-made crystals formed in DMF-H_2O that are in the ZIF-7-I phase are converted to ZIF-7-III during activation. ZIF-7-I (as-made) and ZIF-7-II (postactivation) phases formed in MeOH-DMF at room temperature show rectangular morphology (Figure 5c), while rhombic dodecahedra are formed in DMF at 110–140°C (Figures 5d, e). The hybrid ZIF-7-90 materials with ZIF-7-II crystalline phase formed at room temperature with 70–99% Bz-IM loadings have ill-defined morphologies of small and aggregated crystals (Figures 5g–i), in general agreement with the broad peak shapes observed in the XRD patterns. If the crystallization of ZIF-7-90 hybrids occurs in one solvent, that is, MeOH, the morphology and crystallization are different; the presence of both OHC-IM and BZ-IM linkers in MeOH solution at 90°C forms large particles decorated with the small crystals on the surface introduced as new ZIF-7-90-V phase (Figure 5f). Also, the new phase ZIF-7-90-IV forms in a unique rod-like twinned or intergrown morphology (Figures 5k–l). The ZIF-7-90 frameworks crystallized in the ZIF-90 phase show the typical rhombic dodecahedral shape of the ZIF-90 phase (Figures 5m–o). In general, the average crystal sizes of the hybrid ZIF-7-90 materials formed in DMF-H_2O are larger than those formed in MeOH-DMF. Finally, the XRD and SEM investigations suggest that none of the crystallization products contain physical mixtures of two different types of crystals.

Porosity and textural properties

We used both N_2 and CO_2 physisorption to gain access to the microporosity of all the ZIF hybrid materials, especially those that are close to ZIF-7, which has much smaller pores than ZIF-90. Figures 6a, b show N_2 and CO_2 physisorption isotherms of ZIF-7-90 hybrids, respectively. Supporting Information Figures S3a, b show the surface areas and micropore volumes of activated ZIF-7-90 hybrid materials obtained from these measurements, and the calculated values are also listed in Supporting Information Table S1. The micropore volumes and surface areas decrease which increased Bz-IM inclusion into the ZIF-7-90 frameworks. Among the different phases of hybrid ZIF-7-90, the ZIF-90 phases are the most microporous and the ZIF-7-II phases show the lowest microporosity. The ZIF-7-III phases are not included in this discussion since they are considered dense.[10] However, the new ZIF-7-90-IV phase shows intermediate porosity between the ZIF-7-II and ZIF-90 phases. At 36% Bz-IM loading, the microporosity is decreased by ~50% in comparison with pure ZIF-90. The N_2 physisorption isotherm of ZIF-90 exhibits an inflection point (Figure 6a, IV) with a hysteresis loop at $P/P_0 \sim 0.4$ attributed to constriction in the micropores because of the aldehyde functional groups.[11] The isotherms of the ZIF-90 phase hybrids show two other inflection points: one at $P/P_0 \sim 10^{-5}$ (I), attributed to the permanent microprosity and the other at $P/P_0 \sim 10^{-4}$ (II), due to the "gate-opening" phenomenon that allows access of more N_2 molecules into the micropores *via* linker rotation. When the Bz-IM loading in the framework reaches 40% and produces the new ZIF-7-90-IV phase, these two inflection points are replaced by a single inflection point at $P/P_0 \sim 10^{-3}$ (III). A similar behavior at $P/P_0 \sim 10^{-2}$ (III) also occurs in the hybrids with the ZIF-7-II phase. In both cases, the single low-pressure inflection point is attributed to the permanent microporosity. The bulky Bz-IM linkers limit the linker rotation (and hence gate-opening), thus the gate-opening effect in the ZIF-7-90 hybrid frameworks containing 40–100% Bz-IM loading is severely limited. The microporosity rapidly decreases as the pure ZIF-7-II phase is approached, since the ZIF-7-II pores are too small to be accessible by N_2 at cryogenic conditions. A 50–50 (molar) physical mixture of ZIF-7-II and ZIF-90 crystals was also prepared and analyzed. It is clear that the physical mixture physisorbs higher amounts than the same composition of hybrid ZIF-7_{49}-90_{51}. The inflection points of both ZIF-7-II and ZIF-90 are observed in the N_2 isotherm of the physical mixture, whereas in the 7_{49}-90_{51} hybrid only the inflection point at $P/P_0 \sim 10^{-2}$ can be seen. These results further confirm that we have synthesized true hybrid ZIF-7-90 materials with tunable microporosity different from the pure ZIF-7 and pure ZIF-90 phases.

Figure 6b shows the CO_2 physisorption isotherms of hybrid ZIF-7-90 materials. The isotherm of pure ZIF-7-II phase shows a hysteresis loop similar to the earlier measurements by Bergh et al.[24] and Cai et al.[25] However, ZIF-7-III phase materials did not adsorb CO_2 at 273 K and are considered dense, in agreement with previous works.[10,25] The adsorption and desorption branches of the CO_2 isotherms of the ZIF-7-90 materials with high loadings of OHC-IM (i.e., ZIF-90 phase) are all very similar and show no hysteresis. The strong quadruple moment of CO_2 allows a specific interaction with the OHC-IM linker. As shown in Supporting Information Figure S4, the CO_2 isotherms of the ZIF-7-8 materials show a hysteresis for different compositions while the ZIF-7-90 and ZIF-8-90 materials do not. In general, the CO_2 isotherms at 273 K allow us to measure the total pore volume more accurately but the shapes of the CO_2 isotherms are much less sensitive to the details of the pore structure due to the temperature (273 K) being close to the critical point.

In an earlier study,[5] we showed that the HK[20] equations provided a consistent and physically reasonable method to estimate the PSDs of hybrid ZIF-8-90 and ZIF-7-8. The PSDs obtained cannot be considered as absolute values because of the approximations made in these equations,[26] but they can be used to determine the relative trends in the PSDs of the hybrid ZIF-7-90 materials. Here we used the same physical parameters from our previous N_2 physisorption study of ZIF-8-90 and ZIF-7-8 materials[5] for modeling Bz-IM and OHC-IM linkers, along with N_2 adsorption data points at low relative pressures ($P/P_0 \leq 0.05$). Figure 7 shows the resulting PSD_S for hybrid ZIF-7-90 containing 0-49% Bz-IM. The ZIF-90 phase

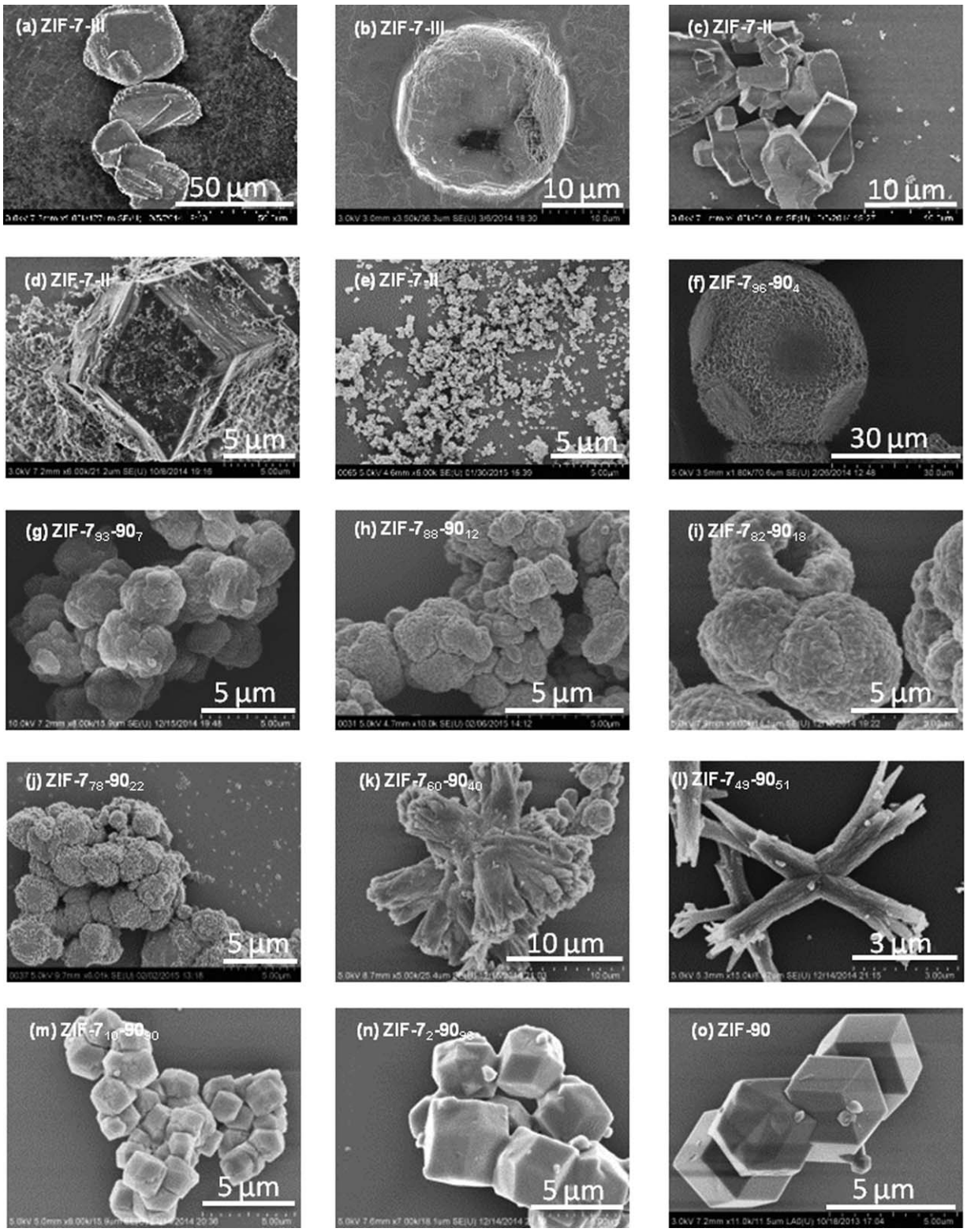

Figure 5. SEM images of activated ZIF-7-90 hybrids at different BZ-IM loadings and synthesized. (a) 100% at 25°C (ZIF-7-III phase); (b) 100% at 90°C (ZIF-7-III phase); (c) 100% at 25°C (ZIF-7-II phase); (d) 100% at 120°C (ZIF-7-II phase); (e) 100% at 140°C (ZIF-7-II phase); (f) 96% at 90°C (ZIF-7-90-V phase); (g) 93% at 25°C (ZIF-7-II phase); (h) 88% at 25°C (ZIF-7-II phase); (i) 82% at 25°C (ZIF-7-II phase); (j) 78% at 25°C (ZIF-7-II phase); (k) 60% at 25°C (ZIF-7-90-IV phase); (l) 49% at 25°C (ZIF-7-90-IV phase); (m) 10% at 25°C (ZIF-90 phase); (n) 2% at 25°C (ZIF-90 phase); and (o) 0% at 25°C (ZIF-90 phase).

materials (0–40% Bz-IM) show two peaks: the primary micropores at ~5 Å and another feature at 6.5 Å attributed to rotation of the linkers (gate-opening). The adsorption capacity of the primary pore size and the intensity of the second feature (gate-opening) decrease as the Bz-IM loading increases because the bulky Bz-IM linkers reduce the microporosity, as

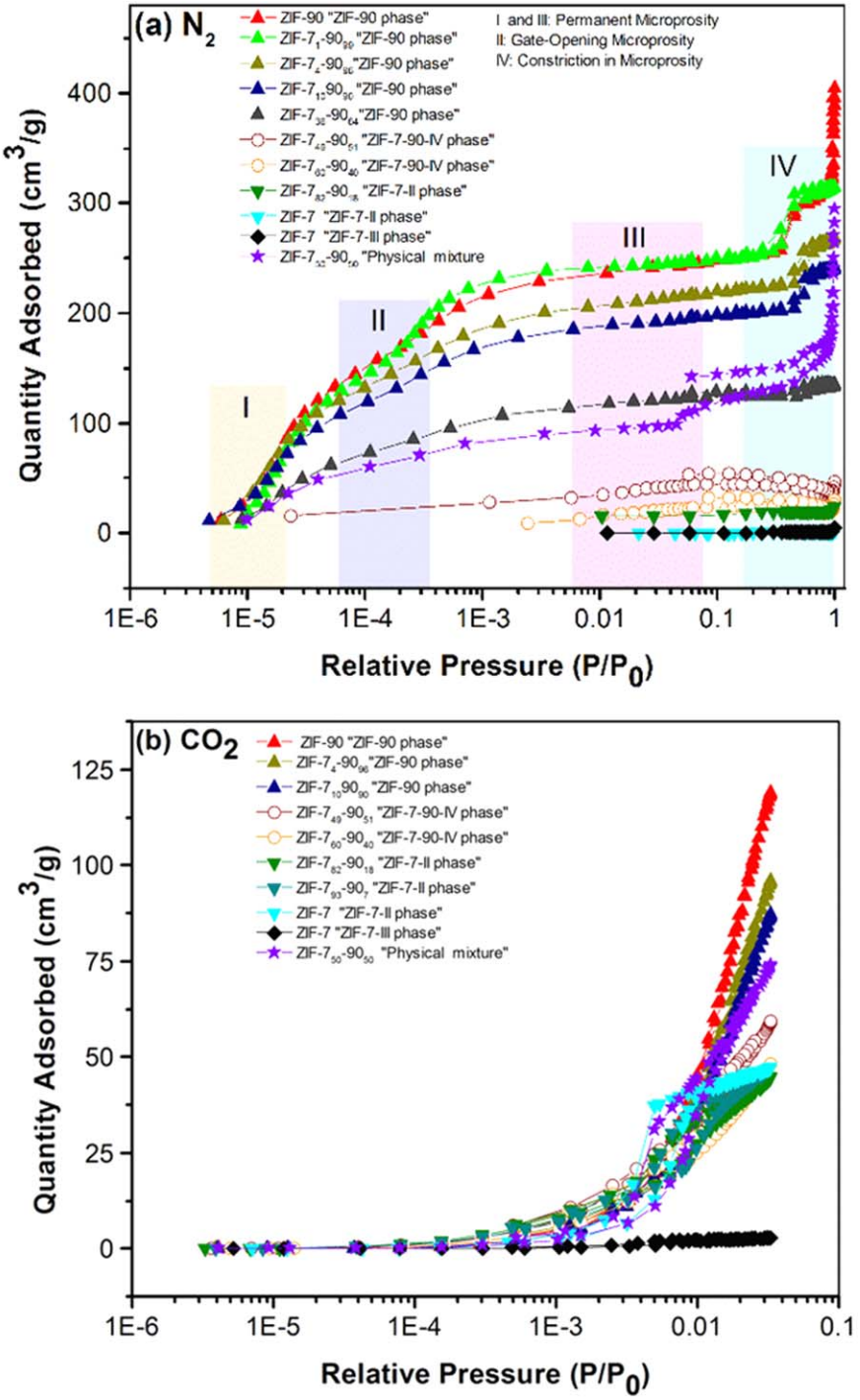

Figure 6. (a) N_2 and (b) CO_2 physisorption isotherms of hybrid ZIF-7-90 materials. Inflection points corresponding to the different microporosity of ZIF-7-90 materials are highlighted with different colors.

[Color figure can be viewed in the online issue, which is available at wileyonlinelibrary.com.]

well as limit or eliminate the gate-opening effect. Next, we applied a DFT model (used widely for adsorption of CO_2 on nanoporous materials such as carbon molecular sieves)[27,28] to model our CO_2 adsorption data and examine the tuning of pore size (Supporting Information Figure S5). The model assumes slit pores and performs non-negative regularization with no smoothing method. The primary pore size values obtained from the DFT model are unphysically large (0.7–0.9 nm) relative to those calculated with the HK method, since the DFT parameters are not quantitatively optimized for CO_2-ZIF interactions. Also, CO_2 physisorption near the critical temperature inhibits the capability of CO_2 molecules to probe small changes in the micropore characteristics.[28] However, Supporting Information Figure S5 clearly shows a trend of increasing primary pore size as well as the appearance of the second (gate-opening) feature as the fraction of the OHC-Im linkers increase. Overall, the physisorption results qualitatively show the tuning of the effective pore size of the hybrid ZIF-7-90 materials, and also demonstrate that the gate-opening effect (and thus the flexibility of the framework) can be tuned. In hybrid ZIF-7-90, more than 50% Bz-IM loading in the framework is required to obtain a rigid structure. In

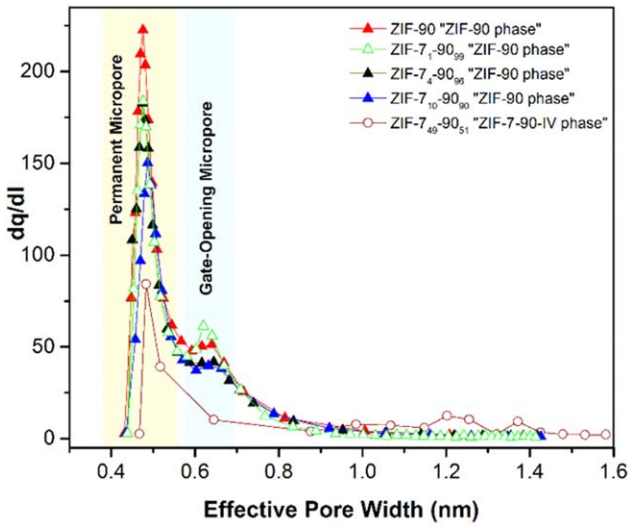

Figure 7. PSDs of hybrid ZIF-7-90 frameworks determined by the HK method.

[Color figure can be viewed in the online issue, which is available at wileyonlinelibrary.com.]

contrast, only 20% Bz-IM loading is required in the hybrid ZIF-7-8 system[5] to suppress the flexibility of the framework and reach a pore size close to that of pure ZIF-7. Thus the hybrid ZIF-7-90 materials considerably expand the range of tunable porosity (over that available using ZIF-8-90 and ZIF-7-8 hybrids) for desired separation applications.

Diffusion and adsorption

To investigate the effects of the tunable pore structure of ZIF-7-90 materials, diffusivity measurements of *n*-butane and *i*-butane were performed. The ZIF-7-III phase materials are nonporous and are not included in these measurements. ZIF-7 has been shown to allow hydrocarbons such as ethane, ethylene, propane, propylene, and butanes into its pores.[9,24] The crystal size limitations of the present ZIF-7-90 materials did not allow us to determine precise diffusion coefficients of the small C_2 and C_3 hydrocarbons because of their relatively fast diffusion in the frameworks. Conversely, the transport (i.e., Fickian) diffusivities of butane isomers could be measured for the ZIF-7-90 materials in the ZIF-7-II, ZIF-7-90-IV, and ZIF-90 phases. Our previously reported volumetric uptake methodology was used. In this method, described in detail elsewhere[17,29] the linear portions of the volumetric uptake curves are fitted with an analytical model for uptake in a sample of given CSD. Figure 8 shows the butane isomer transport diffusivities and the corresponding *n*-butane/*i*-butane diffusion selectivities of the ZIF-7-90 materials at 308 K. The numerical diffusivity values are also listed in Supporting Information Table S2. Although these ZIF-7-90 materials are crystallized in different phases depending on the linker composition, it is clear that tuning of the ZIF-7 linker fraction (x) allows the *i*-butane transport diffusivities to be tuned continuously over 4–5 orders of magnitude. The *n*-butane/*i*-butane diffusion selectivity can be tuned over 4 orders of magnitude. Several differences in butane diffusion behavior are observed in ZIF-7-90 hybrids compared to the recently-investigated ZIF-8-90 hybrids.[17] Materials close to ZIF-7 have low diffusion selectivity (<10) for butane isomers unlike the case of ZIF-8. This is related to the fact that the ZIF-7 pore size is much smaller than that of ZIF-8 and does not allow either isomer to diffuse fast enough. Secondly, the range of *n*-butane diffusivities in the ZIF-7-90 materials is much larger (6–7 orders of magnitude) than in the ZIF-8-90 materials (2 orders of magnitude),[17]

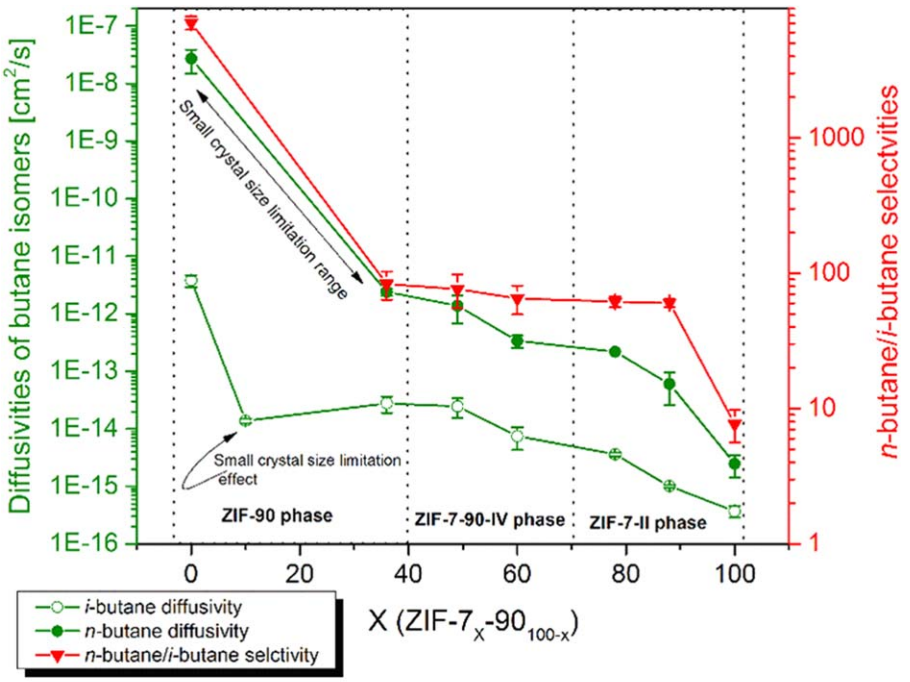

Figure 8. Fickian diffusivities of *n*-butane and *i*-butane (left axis) measured at 308 K and the corresponding *n*-butane/*i*-butane selectivities (right axis) of hybrid ZIF-7-90 materials with varying values of *x* (ZIF-7 linker fraction). The lines connecting the data points are only a guide to the eye. The different crystal phase regions are labeled.

[Color figure can be viewed in the online issue, which is available at wileyonlinelibrary.com.]

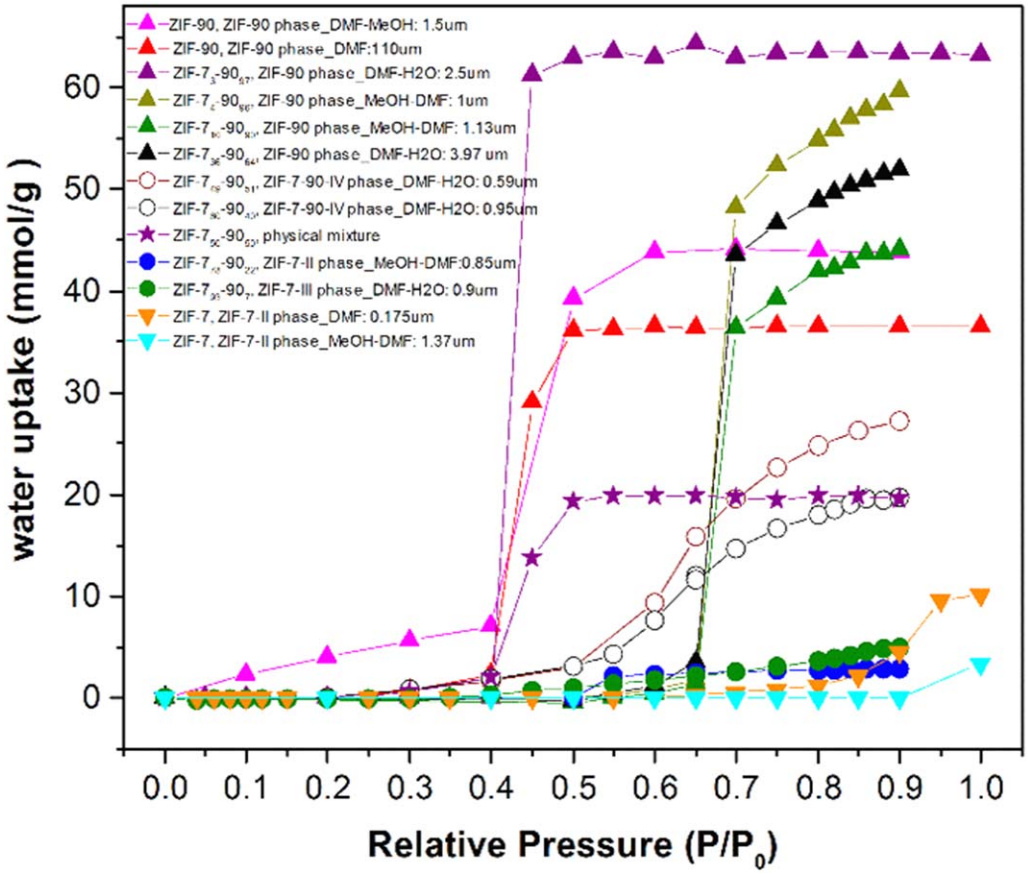

Figure 9. Water adsorption isotherms in hybrid ZIF-7-90 crystals and a 50–50 physical mixture of ZIF-7 and ZIF-90 at 308 K. The *y*-axis is the mmol of water uptake per gm of Zn in the framework.

[Color figure can be viewed in the online issue, which is available at wileyonlinelibrary.com.]

highlighting the expanded tuning of the pore-size range available for hydrocarbon separations using ZIF-7-90 materials.

Water vapor adsorption isotherms of the hybrid ZIF-7-90 materials at 308 K are shown in Figure 9. The two pure ZIF-7-II materials, after activation to remove the guest molecules, are hydrophobic over almost the entire vapor pressure range but adsorb small amounts (3.3–10.0 mmol) of water molecules/gm Zn near the saturation pressure ($P/P_0 \sim 1$). This result corroborates the simulated adsorption data for ZIF-7 reported by Ortiz et al.[30] They found that water adsorption on ZIFs depends not only on the linker in the framework but also on the pore geometry. Thus, even the hydrophobic ZIF materials, such as ZIF-7 and ZIF-8, with the SOD topology have different water adsorption isotherms due to their different pore geometry. Distortion of benzene rings in ZIF-7 forms not only hydrophobic hexagonal windows, but also creates the small hydrophilic sites that can adsorb up to 12 molecules of water.[30] Although the hydrophobicity of the pore walls in materials such as ZIF-7 and ZIF-8 has been shown to enhance water-water hydrogen bonding,[31] the pore geometry remains the main parameter determining water adsorption in ZIF-7. The two ZIF-7-rich mixed-linker materials crystallizing in the ZIF-7-II phase also show hydrophobic behavior as expected. Next, the two materials crystallizing in the new ZIF-7-90-IV phase show increased saturation uptake and a lower uptake pressure $P/P_0 \sim 0.5$, due to the presence of OHC-IM linkers. Furthermore, the isotherms for these materials do not show a very sharp pore-filling transition. While the structure of these materials is yet unknown, the water adsorption isotherms certainly indicate a more porous ZIF structure in relation to the ZIF-7-II phase.

Conversely, the materials crystallizing in the ZIF-90 phase show significant changes in adsorption behavior depending on composition and synthesis solvent system. The two pure ZIF-90 materials have similar uptake pressures of $P/P_0 \sim 0.4$[5,30,32] but show small differences in their approach to the critical filling pressure and their saturation uptake. This illustrates the role of the solvent system, which can be expected to affect the number of defects in the structure as well as residual solvent molecules (especially DMF) even after activation. Similarly, a ZIF-90 rich hybrid with 3% of ZIF-7 linkers (ZIF-7$_3$-90$_{97}$) and made in a DMF-H_2O solvent shows the same pore filling pressure as pure ZIF-90 (as expected) but a larger saturation uptake (presumably because of fewer residual solvent in the pores and more complete activation). For this solvent system, increase in the ZIF-7 linker content to 36% leads to a shift in the filling pressure to $P/P_0 \sim 0.65$ and a lower saturation uptake. Both observations are consistent with the increased hydrophobicity and lower pore volume of the material. However, the two hybrid ZIF-7-90 materials crystallizing in the ZIF-90 phase but made with a MeOH-DMF solvent system show different behavior. The material with 4% ZIF-7 linkers (ZIF-7$_4$-90$_{96}$) is compositionally similar to the ZIF-7$_3-$90$_{97}$ discussed earlier and also tends to a high saturation uptake,

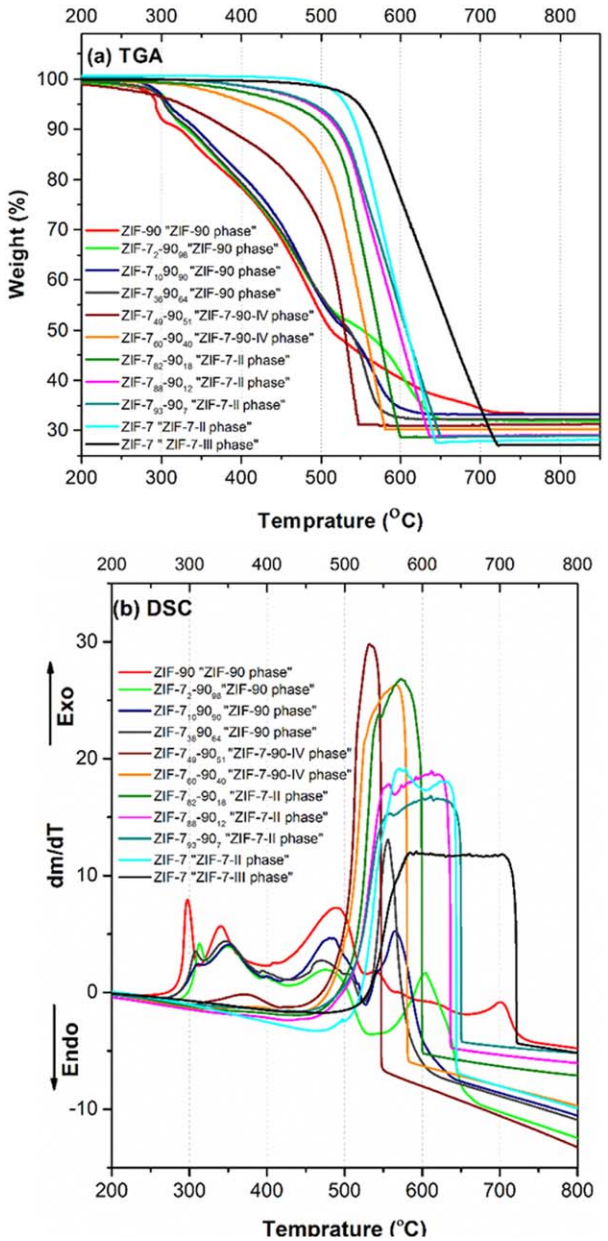

Figure 10. Thermal decomposition analysis of hybrid ZIF-7-90 materials: (a) TGA and (b) DSC curves.

[Color figure can be viewed in the online issue, which is available at wileyonlinelibrary.com.]

but the approach to saturation and the pore-filling pressure ($P/P_0 \sim 0.65$) are very different. The ZIF-$7_{10}-90_{90}$ material displays a lower saturation uptake due to the increased Bz-Im content, but its pore-filling pressure is similar to ZIF-7_4-90_{96}. This indicates that the majority of the pore apertures in these two materials have similar structure and are lined with similar amounts of Bz-Im linkers.

While some of the above discussed effects are not quantitatively understood at present and may require more detailed elucidation that is beyond the scope of this study, it is clear that even small loadings of Bz-IM linker are sufficient to drastically increase the hydrophobicity of the mixed-linker ZIF-7-90 materials while maintaining their ZIF-90 crystal phase. This finding may be useful in applying ZIF-7-90 materials for separation of organic/water mixtures. Finally, a 50–50 (molar) physical mixture of ZIF-7-II and ZIF-90 crystals also behaves quite differently from a hybrid ZIF-7-90 of similar overall composition (51% OHC-IM loading): the physical mixture starts to uptake water at the same pressure as pure ZIF-90 and also adsorbs a lower total amount of water at the saturation pressure. This is additional evidence that the ZIF-7-90 materials are true hybrids and shows that their hydrophilicity can be systematically tuned by changing the linker ratio.

Thermal stability

TGA-DSC analysis was performed to determine the thermal stability of the activated ZIF-7-90 materials (Figures 10a, b). The ZIF-7-III nonporous phase is the most stable and decomposes around 550°C. Pure ZIF-7-II is stable until 500°C, and the hybrid ZIF-7-90 materials crystallized in the ZIF-7-II phase show thermal stability until 400°C. The ZIF-7-90-IV phase hybrids are stable until 300–350°C. The ZIF-90 phase hybrids are only stable up to 300°C, similar to the hybrid ZIF-8-90 materials containing $\geq$50% OHC-IM fractions.[5] Aldehyde groups are easily oxidized in diluted air at higher temperatures, while the aryl groups of Bz-IM provide additional stability and delay the decomposition of the framework to higher temperatures.

Conclusion

We have successfully synthesized and characterized a new set of hybrid ZIFs (namely, ZIF-7-90). ZIF-7-90 synthesis required the detailed exploration of the solvent system and synthesis conditions to successfully produce hybrid ZIFs in the entire compositional range of interest. ZIF-7-90 materials show at least five different crystalline phases, including two new phases not previously reported in pure ZIF-7 and pure ZIF-90 synthesis syntheses. The hybrid ZIF-7-90 materials are shown to allow continuous tuning of textural, adsorption, and diffusion properties over a wide range. Both the water adsorption as well as the butane isomer diffusion behavior of ZIF-7-90 frameworks displays new features in relation to ZIF-8-90 hybrid materials. Overall, hybrid ZIF-7-90 materials significantly expand the range of tunable pore characteristics over ZIF-8-90 and ZIF-7-8 materials.

Acknowledgment

This work was supported by Phillips 66 Company.

Literature Cited

1. Brown AJ, Brunelli NA, Eum K, et al. Interfacial microfluidic processing of metal-organic framework hollow fiber membranes. *Science*. 2014;345(6192):72–75.
2. Park KS, Ni Z, Côté AP, et al. Exceptional chemical and thermal stability of zeolitic imidazolate frameworks. *Proc Natl Acad Sci*. 2006;103(27):10186–10191.
3. Huang A, Dou W, Caro J. Steam-stable zeolitic imidazolate framework ZIF-90 membrane with hydrogen selectivity through covalent functionalization. *J Am Chem Soc*. 2010;132(44):15562–15564.
4. Farha OK, Yazaydın AÖ, Eryazici I, et al. De novo synthesis of a metal–organic framework material featuring ultrahigh surface area and gas storage capacities. *Nat Chem*. 2010;2(11):944–948.
5. Thompson JA, Blad CR, Brunelli NA, et al. Hybrid zeolitic imidazolate frameworks: controlling framework porosity and functionality by mixed-linker synthesis. *Chem Mater*. 2012;24(10):1930–1936.
6. Liu X, Li Y, Ban Y, et al. Improvement of hydrothermal stability of zeolitic imidazolate frameworks. *Chem Commun*. 2013;49(80):9140–9142.

7. Cheng Y, Kajiro H, Noguchi H, et al. Tuning of gate opening of an elastic layered structure MOF in CO_2 sorption with a trace of alcohol molecules. *Langmuir*. 2011;27(11):6905–6909.
8. Fairen-Jimenez D, Moggach SA, Wharmby MT, Wright PA, Parsons S, Düren T. Opening the gate: framework flexibility in ZIF-8 explored by experiments and simulations. *J Am Chem Soc*. 2011; 133(23):8900–8902.
9. Aguado S, Bergeret G, Titus MP, et al. Guest-induced gate-opening of a zeolite imidazolate framework. *New J Chem*. 2011;35(3):546–550.
10. Zhao P, Lampronti GI, Lloyd GO, et al. Phase transitions in zeolitic imidazolate framework 7: the importance of framework flexibility and guest-induced instability. *Chem Mater*. 2014;26(5):1767–1769.
11. Morris W, Doonan CJ, Furukawa H, Banerjee R, Yaghi OM. Crystals as molecules: postsynthesis covalent functionalization of zeolitic imidazolate frameworks. *J Am Chem Soc*. 2008;130(38):12626–12627.
12. Karagiaridi O, Vermeulen NA, Klet RC, et al. Functionalized defects through solvent-assisted linker exchange: synthesis, characterization, and partial postsynthesis elaboration of a metal–organic framework containing free carboxylic acid moieties. *Inorg Chem*. 2015;54(4):1785–1790.
13. Karagiaridi O, Bury W, Mondloch JE, Hupp JT, Farha OK. Solvent-assisted linker exchange: an alternative to the de novo synthesis of unattainable metal–organic frameworks. *Angew Chem Int Ed*. 2014; 53(18):4530–4540.
14. Verduzco JM, Chung H, Hu C, Choe W. Metal−organic framework assembled from T-shaped and octahedral nodes: a mixed-linker strategy to create a rare anatase TiO2 topology. *Inorg Chem*. 2009; 48(19):9060–9062.
15. Zhang C, Xiao Y, Liu D, Yang Q, Zhong C. A hybrid zeolitic imidazolate framework membrane by mixed-linker synthesis for efficient CO2 capture. *Chem Commun*. 2013;49(6):600–602.
16. Thompson JA, Brunelli NA, Lively RP, Johnson J, Jones CW, Nair S. Tunable CO2 adsorbents by mixed-linker synthesis and postsynthetic modification of zeolitic imidazolate frameworks. *J Phys Chem C*. 2013;117(16):8198–8207.
17. Eum K, Jayachandrababu KC, Rashidi F, et al. Highly tunable molecular sieving and adsorption properties of mixed-linker zeolitic imidazolate frameworks. *J Am Chem Soc*. 2015;137(12):4191–4197.
18. Gucuyener C, van den Bergh J, Gascon J, Kapteijn F. Ethane/ethene separation turned on its head: selective ethane adsorption on the metal-organic framework ZIF-7 through a gate-opening mechanism. *J Am Chem Soc*. 2010;132(50):17704–17706.
19. Bae T-H, Lee JS, Qiu W, Koros WJ, Jones CW, Nair S. A high-performance gas-separation membrane containing submicrometer-sized metal–organic framework crystals. *Angew Chem Int Ed*. 2010; 49(51):9863–9866.
20. Horvath G, Kawazoe K. Method for the calculation of effective pore-size distribution in molecular-sieve carbon. *J Chem Eng Jpn*. 1983;16(6):470–475.
21. Zimmerman CM, Singh A, Koros WJ. Diffusion in gas separation membrane materials: a comparison and analysis of experimental characterization techniques. *J Polym Sci Part B: Polym Phys*. 1998; 36(10):1747–1755.
22. Karger J, Ruthven DM, Theodorou DN. *Diffusion in Nanoporous Materials, Vol*. 1, 1st *ed*. Wiley, 2012.
23. Karger J, Binder T, Chmelik C, et al. Microimaging of transient guest profiles to monitor mass transfer in nanoporous materials. *Nat Mater*. 2014;13(4):333–343.
24. van den Bergh J, Gücüyener C, Pidko EA, Hensen EJM, Gascon J, Kapteijn F. Understanding the anomalous alkane selectivity of ZIF-7 in the separation of light alkane/alkene mixtures. *Chemistry*. 2011; 17(32):8832–8840.
25. Cai W, Lee T, Lee M, et al. Thermal structural transitions and carbon dioxide adsorption properties of zeolitic imidazolate framework-7 (ZIF-7). *J Am Chem Soc*. 2014;136(22):7961–7971.
26. Thommes M. Introduction to zeolite science and practice. In: Cejka J, van Bekkum H, Corma A, Schüth F, editors. *Studies in Surface Science and Catalysts, Vol*. 168. 2007:495–525.
27. Tarazona P. Free-energy density functional for hard spheres. *Phys Rev A*. 1985;31(4):2672–2679.
28. Tarazona P, Marconi UMB, Evans R. Phase equilibria of fluid interfaces and confined fluids. *Mol Phys*. 1987;60(3):573–595.
29. Zhang C, Lively RP, Zhang K, Johnson JR, Karvan O, Koros WJ. Unexpected molecular sieving properties of zeolitic imidazolate framework-8. *J Phys Chem Lett*. 2012;3(16):2130–2134.
30. Ortiz AU, Freitas AP, Boutin A, Fuchs AH, Coudert FX. What makes zeolitic imidazolate frameworks hydrophobic or hydrophilic? The impact of geometry and functionalization on water adsorption. *Phys Chem Chem Phys*. 2014;16(21):9940–9949.
31. Gomez-Alvarez P, Calero S. Insights into the microscopic behaviour of nanoconfined water: host structure and thermal effects. *CrystEngComm*. 2015;17(2):412–421.
32. Zhang K, Lively RP, Dose ME, et al. Alcohol and water adsorption in zeolitic imidazolate frameworks. *Chem Commun*. 2013;49(31): 3245–3247.

Manuscript received Aug. 3, 2015, and revision received Oct. 11, 2015.